JOURNAL OF THERMOPHYSICS AND HEAT TRANSFER
Vol. 24, No. 1, January–March 2010

# Vibrational Modeling of $CO_2$ in High-Enthalpy Nozzle Flows

Sriram Doraiswamy*
*University of Minnesota, Minneapolis, Minnesota 55455*
J. Daniel Kelley†
*University of Missouri—St. Louis, St. Louis, Missouri 63121-4400*
and
Graham V. Candler‡
*University of Minnesota, Minneapolis, Minnesota 55455*

DOI: 10.2514/1.43280

**A state-specific vibrational model for $CO_2$, CO, $O_2$, and O systems is devised by taking into account the first few vibrational states of each species. All vibrational states with energies at or below 1 eV are included in the present work. Of the three modes of vibration in $CO_2$, the antisymmetric mode is considered separately from the symmetric stretching mode and the doubly degenerate bending modes. The symmetric and bending modes are grouped together because the energy transfer rates between the two modes are very large due to Fermi resonance. The symmetric and bending modes are assumed to be in equilibrium with the translational and rotational modes. The kinetic rates for the vibrational-translation energy exchange reactions and the intermolecular and intramolecular vibrational-vibrational energy exchange reactions are based on experimental data to the maximum extent possible. Extrapolation methods are employed when necessary. This vibrational model is then coupled with an axisymmetric computational fluid dynamics code to study the expansion of $CO_2$ in a nozzle.**

## I. Introduction

THE present work is an ongoing research effort aimed at addressing the issue of increased shock standoff distance observed in the high-enthalpy (5 MJ/kg) $CO_2$ runs at the Calspan-University of Buffalo Research Center (CUBRC) Large-Enthalpy National Shock (LENS) hypersonic facility [1]. The observed shock standoff distance was more than twice the value predicted by computational fluid dynamics (CFD). A systematic study was undertaken in [1] to investigate the reason behind this anomalous behavior by freezing vibrational and chemical energy in the expanding flow inside the nozzle. This numerical experiment was carried out find the effect of the internal energy on shock standoff distance and is not based on physics. It was found that the frozen vibrational energy had a much larger impact on the shock standoff distance than the frozen chemical energy. In the previous study [1], a frozen vibrational content of 42% of the total enthalpy was found to predict the shock shape correctly and to improve the quality of agreement of surface pressure measurements and heat transfer rates. Though the vibrational content of 42% is aphysical, it does show that there is a need to better model the vibrational processes such as intermolecular $V$-$V$ exchange, intramolecular $V$-$V$ exchange, and $V$-$T$ exchange reactions. There is a large body of literature regarding the vibrational energy transfer in $CO_2$, both intramolecular transfer among the internal state manifolds and intermolecular transfer processes to other molecules, including CO and $O_2$. Representative collections of such data are found in the surveys by Taylor and Bitterman [2], Lewis and Trainor [3], and Weitz and Flynn [4]. Much of the interest in $CO_2$ stems from its value as a laser medium. Efforts to model such lasers (which typically use $CO_2$, $N_2$, $O_2$, and He) have employed reduced-reaction sets with success [5]. Given the similarity of the high-enthalpy $CO_2$ ($CO_2$, CO, and $O_2$) to the laser system, one can be optimistic that our rate equation calculation will point to a simplified approach. The goal is to develop a simplified model with a few characteristic temperatures that will greatly condense the rate data. This cannot be done without explicit calculations that justify such simplification.

Presented as Paper 1570 at the 47th AIAA Aerospace Sciences Meeting, Orlando, FL, 5–9 January 2009; received 16 January 2009; revision received 15 July 2009; accepted for publication 15 July 2009. 

*Graduate Student, Department of Aerospace Engineering and Mechanics. Student Member AIAA.
†Adjunct Professor, Department of Physics and Astronomy. Senior Member AIAA.
‡Professor, Department of Aerospace Engineering and Mechanics. Fellow AIAA.

## II. Vibrational Modeling of $CO_2$

### A. Thermodynamic Calculations

The STANJAN thermodynamic package was used to calculate the reservoir gas properties for run 8 as described by MacLean and Holden [1]. Run 8 was one of several tests run at the CUBRC for high-enthalpy high-density $CO_2$ gas. Similar calculation with a different thermodynamics package has been reported by MacLean and Holden, and the results of the two codes were in good agreement. Table 1 shows the computed reservoir conditions for run 8 such as temperature, density, and mass fractions for different species. The excited electronic $O_2$ states are not included; their effect on the expansion would be to increase the amount of unrelaxed enthalpy by a few percent in the freestream.

The results in Table 1 are used to compute the number densities in each vibrational state for $CO_2$, CO, and $O_2$. In general, for a given species, the population $N_i$ in the level $i$ relative to that in the ground state $N_0$ is given by

$$\frac{N_i}{N_0} = \left(\frac{g_i}{g_0}\right) \exp\left(-\frac{\Delta E_i}{kT}\right) \tag{1}$$

where $g_i$ is the statistical weight of level $i$, $\Delta E_i$ is the energy of level $i$ above the ground state, $k$ is the Boltzmann constant, and $T$ is the temperature. The total population in all the states is

$$N_{\text{total}} = N_0 + N_1 + N_2 + \cdots = N_0\left(1 + \Sigma\left[\frac{g_i}{g_0}\exp\left(-\frac{\Delta E_i}{kT}\right)\right]\right) \tag{2}$$

where the sum is over all levels from $i = 1$ to a level high enough that succeeding terms are essentially zero. For a temperature of 3500 K and energy of 8000 $\text{cm}^{-1}$, the exponential term in Eq. (2) has a value

**Table 1 Reservoir conditions for the CUBRC run with an effective enthalpy of 5.63 MJ/kg and a pressure of 29.5 MPa**

| Condition | Value |
|---|---|
| Temperature | 3500 K |
| $\rho$ | 39.9 kg/m$^3$ |
| $c\mathrm{CO_2}$ | 0.7737 |
| $c\mathrm{CO}$ | 0.1440 |
| $c\mathrm{O_2}$ | 0.0786 |
| $c\mathrm{O}$ | 0.0036 |

of 0.037. The statistical weights $g_i$ are unity for CO and $O_2$ vibrational levels and for the $CO_2$ antisymmetric stretch levels considered here. This fact coupled with the small value of the exponential term at 8000 cm$^{-1}$ indicates that neglect of higher energy levels in these manifolds would have little effect on the computed populations.

The stretch-bend manifold of $CO_2$ states receives special treatment in obtaining the state-specific population of the antisymmetric states. The first simplification is to group the symmetric stretch $\nu_1$ and bending modes $\nu_2$ of $CO_2$, because they form a set of levels that are strongly coupled by collisions with other molecules [6] and by Fermi resonance among themselves. Given the efficient intergroup coupling, it is reasonable to label the symmetric stretch-bend levels with a single-quantum number $\nu_{\mathrm{SB}}$ and to consider them separately from the antisymmetric stretch mode $\nu_3$. An additional simplification is realized using the fact that the collisional deactivation of the stretch-bend states is fast: faster than the rate of energy transfer into them [7]. It is shown that collisional deactivation of the stretch-bend states has a rate constant $k \geq 2$–$3 \times 10^{-12}$ cm$^3$/s at 2000 K and the rate increases for higher stretch-bend states [8,9]. The rate of transfer from the antisymmetric state into the stretch-bend manifold (from $\nu_3 = 1$ to $\nu_2 = 3$), although fairly fast [9], is 5 times slower than the stretch-bend mode $V$-$T, R$ quenching rate and at least 15 times slower than transfer out of the $\nu_2 = 3$ state. As the $CO_2$ system relaxes during the expansion, energy transfer from the antisymmetric state collisionally populates the stretch-bend manifold. Because this intramolecular transfer is slower than the stretch-bend manifold relaxation rate via $V$-$T, R$ transfer, the intramolecular process effectively deactivates the antisymmetric state to the heat bath. Further justification for this assumption is given in [1]; this numerical kinetic study of the CUBRC expansion nozzle (run 8) showed that the stretch-bend vibrational temperature was only a few degrees higher than the gas kinetic temperature. The result of all of this is that the stretch-bend manifold is not explicitly treated in this work. The antisymmetric populations $\nu_3$ are implicitly summed over the stretch-bend states. This is analogous to the summation over rotational states for the diatomics. Just as for rotation, the stretch-bend manifold is assumed to be at the gas kinetic temperature throughout the expansion. A similar state-specific approach for $CO_2$ was carried out by Limbaugh and Drakes [10] to analyze radiatively heated wind tunnels. By construction, the number densities calculated via Eqs. (1) and (2) necessarily sum to the thermodynamically calculated total values obtained from Table 1. Correct ratios among the number densities appropriate to the thermal equilibrium are also obtained. This means that the value in each retained level is a bit higher than the value that would result if more levels were included. For CO and $O_2$, these population differences are less than 1%. For $CO_2(\nu_3)$, the difference is about 2%. With the 8000 cm$^{-1}$ limit given previously, there will be four $CO_2(\nu_3)$ levels, five CO levels, and six $O_2$ levels, including the ground states. Along with the O atoms, there are a total of 16 separate species. The resulting populations are shown in Table 2.

**Table 2 Number densities for individual species in the reservoir**

| Species | Number densities, cm$^{-3}$ |
|---|---|
| Total $CO_2(\nu_3)$ | $\mathbf{4.220^{20}}$ |
| $\nu_3 = 0$ | $2.660^{20}$ |
| $\nu_3 = 1$ | $1.020^{20}$ |
| $\nu_3 = 2$ | $0.391^{20}$ |
| $\nu_3 = 3$ | $0.152^{20}$ |
| Total $CO_2$ | $\mathbf{1.240^{20}}$ |
| $v = 0$ | $0.730^{20}$ |
| $v = 1$ | $0.302^{20}$ |
| $v = 2$ | $0.127^{20}$ |
| $v = 3$ | $0.054^{20}$ |
| $v = 4$ | $0.023^{20}$ |
| Total $O_2$ | $\mathbf{5.900^{19}}$ |
| $v = 0$ | $2.830^{19}$ |
| $v = 1$ | $1.490^{19}$ |
| $v = 2$ | $0.794^{19}$ |
| $v = 3$ | $0.429^{19}$ |
| $v = 4$ | $0.234^{19}$ |
| $v = 5$ | $0.129^{19}$ |
| Total O | $\mathbf{5.400^{18}}$ |

### B. Vibrational Energy Transfer Processes

Although energy transfer data are available for the species of interest, most involve the $v = 1 \rightarrow 0$ transition and limited temperature ranges. We will be required to scale the data to higher states by applying factors derived from transition matrix elements and by adjusting the rate constant to account for the varying energy defects between initial and final vibrational states. First, we discuss the transition matrix elements. The collisional interactional potential can be formally written as

$$V_I(R, r_1, r_2) = (1 + a\delta r_2 + b\delta r_2 + c\delta r_1\delta r_2 + d\delta r_1^2 + e\delta r_1^2 + \cdots)V_I(R, r_1^0, r_2^0) \tag{3}$$

The $R$ coordinate describes relative motion between two colliding molecules and contains the angular information as well. The $\delta r$ are the small displacements of the molecular internal separation from the equilibrium values $r^0$. The expansion of the right-hand side of Eq. (3) can be terminated at second order with little loss in accuracy. The two linear $\delta r$ terms in the interaction potential are responsible for excitation/deexcitation of vibration in molecules 1 and 2, respectively, (i.e., single molecule $V$-$T, R$ processes). The bilinear term is responsible for the $V$-$V$ transfer, and the quadratic terms produce two-quantum processes in molecule 1 or 2. The bilinear term can also produce simultaneous excitation in molecules 1 and 2. The two-quantum process can be ignored in our system, because the one-quantum energies are high ($\sim$2000 cm$^{-1}$) and the two-quantum processes at $\sim$4000 cm$^{-1}$ are much less probable, even at the temperatures in the present study. If the molecules are harmonic oscillators, the single-quantum transition probabilities for a given molecule scale with the upper state quantum number; a $2 \rightarrow 1$ process has twice the probability of a $1 \rightarrow 0$ process. This scaling rule remains a good approximation for the real anharmonic molecules in the $CO_2$–CO–$O_2$ system, because the anharmonic effects are small for the relevant low-lying states. Thus, we will use this scaling to extrapolate rate constants from lower to higher states.

A more complicated scaling involves accounting for the varying state energy separations resulting from anharmonicity. A complete treatment of the energy-averaged set of molecular collisions interacting through $V_I$ in Eq. (3) leads to a rate constant for a given process. To do this exactly, one must have complete knowledge of $V_I$ and then execute a quantum-mechanical treatment of the dynamics. This has been done only for a few systems, and the results are numerical and not analytical. However, various approximate approaches have been developed that give useful results, although arbitrary adjustments and constants are employed to get agreement with experiment. The best known of these analytical treatment is the method of Schwartz–Slawsky–Herzfeld (SSH) theory, as described in [11]. The key aspect of this theory that we use here is the prediction, in its simplest form, of a rate-constant expression:

$$k_f = C \exp(B/T^{1/3}) \tag{4}$$

where $B$ is a function of the transition frequency $\nu$ raised to the two-thirds power. In fact, for most of the processes of interest here, the functional form in Eq. (4) provides a good fit to the experimental data, particularly for the temperatures above 500 K. This form has been used for all the $V$-$T, R$ processes and nonresonant $V$-$V$ processes, and the $\nu^{2/3}$ scaling has been used for these $V$-$V$ processes. This $\nu^{2/3}$ scaling has been ignored for the $V$-$T, R$ processes, because the transition frequency variation (a few tens of wave numbers) is not important when applied to the large $V$-$T, R$ frequencies. It does have an effect on the much smaller $V$-$V$ transition frequencies. To summarize, the harmonic oscillator scaling rule is consistently applied to obtain rate constants for higher states from the lower-state experimental values. The SSH frequency scaling is applied only to nonresonant $V$-$V$ processes.

Near-resonant same-species rate constants are treated differently using an approach developed for the CO–CO $V$-$V$ transfer [12]. There are no data for such fast processes at high temperature, and so extrapolation is required. These processes are all fast and do not add or take away much energy from the system. The extrapolated rate constants may not be accurate even within a factor of 2 or 3, but this will have little effect on the flow dynamics.

The rate constants used in the present work are tabulated in Tables 3–5. All the reactions are in the exothermic direction. For the $V$-$T, R$ processes and intermolecular $V$-$V$ processes, the forward rate constants are of the form described in Eq. (4), and for the intramolecular processes, the rate constant is of the form

$$k_f = C(T/1000) \tag{5}$$

The reverse rates are obtained by detailed balance [i.e., multiplying the listed rate constants by $\exp(-\Delta E/kT)$]:

$$k_b = k_f \exp(-\Delta E/kT) \tag{6}$$

The $\Delta E$ values are obtained from spectroscopic data for the molecules involved [21,22] and include anharmonicity corrections. The value of the Boltzmann constant $k$ when $\Delta E$ is expressed in $\mathrm{cm}^{-1}$ is 0.695.

In Table 3, for the reaction

$$\mathrm{CO}_2(\nu_3) + M \rightleftharpoons \mathrm{CO}_2(\nu_3 - 1) + M \tag{7}$$

direct one-quantum $V$-$T$ transfer is certainly very slow and has never been measured. The major $\nu_3$ loss process is intramolecular $V$-$V$ transfer to the stretch-bend manifold. Deactivation of the stretch-bend manifold is fast at temperatures and densities appropriate for this study, and it can be safely be treated as part of the heat bath with the rotational modes. Therefore, the intramolecular $V$-$V$ process is

**Table 3 Rate constants for $V$-$T, R$ processes**

| Reaction | $C$, $\mathrm{cm}^3/\mathrm{s}$ | $B$ | $\Delta E$, $\mathrm{cm}^{-1}$ | Source |
|---|---|---|---|---|
| $\mathrm{CO}(v=1) + \mathrm{O} \rightleftharpoons \mathrm{CO}(v=0) + \mathrm{O}$ | $2.50^{-6}$ | −168 | 2143 | [13,14] |
| $\mathrm{CO}(v=2) + \mathrm{O} \rightleftharpoons \mathrm{CO}(v=1) + \mathrm{O}$ | $5.00^{-6}$ | −168 | 2116 | [a] |
| $\mathrm{CO}(v=3) + \mathrm{O} \rightleftharpoons \mathrm{CO}(v=2) + \mathrm{O}$ | $7.50^{-6}$ | −168 | 2089 | [a] |
| $\mathrm{CO}(v=4) + \mathrm{O} \rightleftharpoons \mathrm{CO}(v=3) + \mathrm{O}$ | $1.00^{-5}$ | −168 | 2063 | [a] |
| $\mathrm{CO}(v=1) + \Sigma\mathrm{CO}_2 \rightleftharpoons \mathrm{CO}(v=0) + \Sigma\mathrm{CO}_2$ | $1.20^{-6}$ | −240 | 2143 | [15] |
| $\mathrm{CO}(v=2) + \Sigma\mathrm{CO}_2 \rightleftharpoons \mathrm{CO}(v=1) + \Sigma\mathrm{CO}_2$ | $2.40^{-6}$ | −240 | 2116 | [a] |
| $\mathrm{CO}(v=3) + \Sigma\mathrm{CO}_2 \rightleftharpoons \mathrm{CO}(v=2) + \Sigma\mathrm{CO}_2$ | $3.60^{-6}$ | −240 | 2089 | [a] |
| $\mathrm{CO}(v=4) + \Sigma\mathrm{CO}_2 \rightleftharpoons \mathrm{CO}(v=3) + \Sigma\mathrm{CO}_2$ | $4.80^{-6}$ | −240 | 2063 | [a] |
| $\mathrm{CO}(v=1) + \Sigma\mathrm{CO} \rightleftharpoons \mathrm{CO}(v=0) + \Sigma\mathrm{CO}$ | $1.20^{-6}$ | −240 | 2143 | [a] |
| $\mathrm{CO}(v=2) + \Sigma\mathrm{CO} \rightleftharpoons \mathrm{CO}(v=1) + \Sigma\mathrm{CO}$ | $2.40^{-6}$ | −240 | 2116 | [a] |
| $\mathrm{CO}(v=3) + \Sigma\mathrm{CO} \rightleftharpoons \mathrm{CO}(v=2) + \Sigma\mathrm{CO}$ | $3.60^{-6}$ | −240 | 2089 | [a] |
| $\mathrm{CO}(v=4) + \Sigma\mathrm{CO} \rightleftharpoons \mathrm{CO}(v=3) + \Sigma\mathrm{CO}$ | $4.80^{-6}$ | −240 | 2063 | [a] |
| $\mathrm{CO}(v=1) + \Sigma\mathrm{O}_2 \rightleftharpoons \mathrm{CO}(v=0) + \Sigma\mathrm{O}_2$ | $1.20^{-6}$ | −240 | 2143 | [a] |
| $\mathrm{CO}(v=2) + \Sigma\mathrm{O}_2 \rightleftharpoons \mathrm{CO}(v=1) + \Sigma\mathrm{O}_2$ | $2.40^{-6}$ | −240 | 2116 | [a] |
| $\mathrm{CO}(v=3) + \Sigma\mathrm{O}_2 \rightleftharpoons \mathrm{CO}(v=2) + \Sigma\mathrm{O}_2$ | $3.60^{-6}$ | −240 | 2089 | [a] |
| $\mathrm{CO}(v=4) + \Sigma\mathrm{O}_2 \rightleftharpoons \mathrm{CO}(v=3) + \Sigma\mathrm{O}_2$ | $4.80^{-6}$ | −240 | 2063 | [a] |
| $\mathrm{O}_2(v=1) + \mathrm{O} \rightleftharpoons \mathrm{O}_2(v=0) + \mathrm{O}$ | $3.40^{-9}$ | −67.5 | 1556 | [16,17] |
| $\mathrm{O}_2(v=2) + \mathrm{O} \rightleftharpoons \mathrm{O}_2(v=1) + \mathrm{O}$ | $6.80^{-9}$ | −67.5 | 1532 | [a] |
| $\mathrm{O}_2(v=3) + \mathrm{O} \rightleftharpoons \mathrm{O}_2(v=2) + \mathrm{O}$ | $1.02^{-8}$ | −67.5 | 1508 | [a] |
| $\mathrm{O}_2(v=4) + \mathrm{O} \rightleftharpoons \mathrm{O}_2(v=3) + \mathrm{O}$ | $1.36^{-8}$ | −67.5 | 1484 | [a] |
| $\mathrm{O}_2(v=1) + \Sigma\mathrm{CO}_2 \rightleftharpoons \mathrm{O}_2(v=0) + \Sigma\mathrm{CO}_2$ | $3.60^{-7}$ | −190 | 1556 | [15] |
| $\mathrm{O}_2(v=2) + \Sigma\mathrm{CO}_2 \rightleftharpoons \mathrm{O}_2(v=1) + \Sigma\mathrm{CO}_2$ | $7.20^{-7}$ | −190 | 1532 | [a] |
| $\mathrm{O}_2(v=3) + \Sigma\mathrm{CO}_2 \rightleftharpoons \mathrm{O}_2(v=2) + \Sigma\mathrm{CO}_2$ | $1.08^{-6}$ | −190 | 1508 | [a] |
| $\mathrm{O}_2(v=4) + \Sigma\mathrm{CO}_2 \rightleftharpoons \mathrm{O}_2(v=3) + \Sigma\mathrm{CO}_2$ | $1.44^{-6}$ | −190 | 1484 | [a] |
| $\mathrm{O}_2(v=1) + \Sigma\mathrm{CO} \rightleftharpoons \mathrm{O}_2(v=0) + \Sigma\mathrm{CO}$ | $3.60^{-7}$ | −190 | 1556 | [a] |
| $\mathrm{O}_2(v=2) + \Sigma\mathrm{CO} \rightleftharpoons \mathrm{O}_2(v=1) + \Sigma\mathrm{CO}$ | $7.20^{-7}$ | −190 | 1532 | [a] |
| $\mathrm{O}_2(v=3) + \Sigma\mathrm{CO} \rightleftharpoons \mathrm{O}_2(v=2) + \Sigma\mathrm{CO}$ | $1.08^{-6}$ | −190 | 1508 | [a] |
| $\mathrm{O}_2(v=4) + \Sigma\mathrm{CO} \rightleftharpoons \mathrm{O}_2(v=3) + \Sigma\mathrm{CO}$ | $1.44^{-6}$ | −190 | 1484 | [a] |
| $\mathrm{O}_2(v=1) + \Sigma\mathrm{O}_2 \rightleftharpoons \mathrm{O}_2(v=0) + \Sigma\mathrm{O}_2$ | $3.60^{-7}$ | −190 | 1556 | [a] |
| $\mathrm{O}_2(v=2) + \Sigma\mathrm{O}_2 \rightleftharpoons \mathrm{O}_2(v=1) + \Sigma\mathrm{O}_2$ | $7.20^{-7}$ | −190 | 1532 | [a] |
| $\mathrm{O}_2(v=3) + \Sigma\mathrm{O}_2 \rightleftharpoons \mathrm{O}_2(v=2) + \Sigma\mathrm{O}_2$ | $1.08^{-6}$ | −190 | 1508 | [a] |
| $\mathrm{O}_2(v=4) + \Sigma\mathrm{O}_2 \rightleftharpoons \mathrm{O}_2(v=3) + \Sigma\mathrm{O}_2$ | $1.44^{-6}$ | −190 | 1484 | [a] |
| $\mathrm{CO}_2(\nu_3=1) + \Sigma\mathrm{CO}_2 \rightleftharpoons \mathrm{CO}_2(\nu_3=0) + \Sigma\mathrm{CO}_2$ | $3.10^{-10}$ | −80.6 | 2349 | [9] |
| $\mathrm{CO}_2(\nu_3=2) + \Sigma\mathrm{CO}_2 \rightleftharpoons \mathrm{CO}_2(\nu_3=1) + \Sigma\mathrm{CO}_2$ | $6.20^{-10}$ | −80.6 | 2324 | [a] |
| $\mathrm{CO}_2(\nu_3=3) + \Sigma\mathrm{CO}_2 \rightleftharpoons \mathrm{CO}_2(\nu_3=2) + \Sigma\mathrm{CO}_2$ | $9.30^{-10}$ | −80.6 | 2299 | [a] |
| $\mathrm{CO}_2(\nu_3=1) + \Sigma\mathrm{CO} \rightleftharpoons \mathrm{CO}_2(\nu_3=0) + \Sigma\mathrm{CO}$ | $2.10^{-12}$ | −46.1 | 2349 | [a] |
| $\mathrm{CO}_2(\nu_3=2) + \Sigma\mathrm{CO} \rightleftharpoons \mathrm{CO}_2(\nu_3=1) + \Sigma\mathrm{CO}$ | $4.20^{-12}$ | −46.1 | 2324 | [a] |
| $\mathrm{CO}_2(\nu_3=3) + \Sigma\mathrm{CO} \rightleftharpoons \mathrm{CO}_2(\nu_3=2) + \Sigma\mathrm{CO}$ | $6.30^{-12}$ | −46.1 | 2299 | [a] |
| $\mathrm{CO}_2(\nu_3=1) + \Sigma\mathrm{O}_2 \rightleftharpoons \mathrm{CO}_2(\nu_3=0) + \Sigma\mathrm{O}_2$ | $1.25^{-12}$ | −4.6 | 2349 | [a] |
| $\mathrm{CO}_2(\nu_3=2) + \Sigma\mathrm{O}_2 \rightleftharpoons \mathrm{CO}_2(\nu_3=1) + \Sigma\mathrm{O}_2$ | $2.50^{-12}$ | −4.6 | 2324 | [a] |
| $\mathrm{CO}_2(\nu_3=3) + \Sigma\mathrm{O}_2 \rightleftharpoons \mathrm{CO}_2(\nu_3=2) + \Sigma\mathrm{O}_2$ | $3.75^{-12}$ | −4.6 | 2299 | [a] |
| $\mathrm{CO}_2(\nu_3=1) + \mathrm{O} \rightleftharpoons \mathrm{CO}_2(\nu_3=0) + \mathrm{O}$ | $6.25^{-13}$ | 0 | 2349 | [a] |
| $\mathrm{CO}_2(\nu_3=2) + \mathrm{O} \rightleftharpoons \mathrm{CO}_2(\nu_3=1) + \mathrm{O}$ | $1.25^{-12}$ | 0 | 2324 | [a] |
| $\mathrm{CO}_2(\nu_3=3) + \mathrm{O} \rightleftharpoons \mathrm{CO}_2(\nu_3=2) + \mathrm{O}$ | $1.87^{-12}$ | 0 | 2299 | [a] |

[a]Extrapolated data from experiments.

**Table 4 Rate constants for intermolecular *V-V* processes**

| Reaction | $C$, cm$^3$/s | $B$ | $\Delta E$, cm$^{-1}$ | Source |
|---|---|---|---|---|
| $CO_2(\nu_3 = 1) + CO(v = 0) \rightleftharpoons CO_2(\nu_3 = 0) + CO(v = 1)$ | $9.40^{-12}$ | −30.12 | 206 | [18,19] |
| $CO_2(\nu_3 = 2) + CO(v = 0) \rightleftharpoons CO_2(\nu_3 = 1) + CO(v = 1)$ | $1.90^{-11}$ | −27.60 | 181 | [a] |
| $CO_2(\nu_3 = 3) + CO(v = 0) \rightleftharpoons CO_2(\nu_3 = 2) + CO(v = 1)$ | $2.80^{-11}$ | −25.00 | 156 | [a] |
| $CO_2(\nu_3 = 1) + CO(v = 1) \rightleftharpoons CO_2(\nu_3 = 0) + CO(v = 2)$ | $1.90^{-11}$ | −32.70 | 233 | [a] |
| $CO_2(\nu_3 = 2) + CO(v = 1) \rightleftharpoons CO_2(\nu_3 = 1) + CO(v = 2)$ | $3.80^{-11}$ | −30.31 | 208 | [a] |
| $CO_2(\nu_3 = 3) + CO(v = 1) \rightleftharpoons CO_2(\nu_3 = 2) + CO(v = 2)$ | $5.60^{-11}$ | −27.90 | 183 | [a] |
| $CO_2(\nu_3 = 1) + CO(v = 2) \rightleftharpoons CO_2(\nu_3 = 0) + CO(v = 3)$ | $2.80^{-11}$ | −35.2 | 260 | [a] |
| $CO_2(\nu_3 = 2) + CO(v = 2) \rightleftharpoons CO_2(\nu_3 = 1) + CO(v = 3)$ | $5.60^{-11}$ | −32.9 | 235 | [a] |
| $CO_2(\nu_3 = 3) + CO(v = 2) \rightleftharpoons CO_2(\nu_3 = 2) + CO(v = 3)$ | $8.50^{-11}$ | −30.5 | 210 | [a] |
| $CO_2(\nu_3 = 1) + CO(v = 3) \rightleftharpoons CO_2(\nu_3 = 0) + CO(v = 4)$ | $3.80^{-11}$ | −37.6 | 287 | [a] |
| $CO_2(\nu_3 = 2) + CO(v = 3) \rightleftharpoons CO_2(\nu_3 = 1) + CO(v = 4)$ | $7.50^{-11}$ | −35.4 | 262 | [a] |
| $CO_2(\nu_3 = 3) + CO(v = 3) \rightleftharpoons CO_2(\nu_3 = 2) + CO(v = 4)$ | $1.10^{-10}$ | −33.1 | 237 | [a] |
| $CO(v = 1) + O_2(v = 0) \rightleftharpoons CO(v = 0) + O_2(v = 1)$ | $3.50^{-10}$ | −124.0 | 587 | [18,19] |
| $CO(v = 2) + O_2(v = 0) \rightleftharpoons CO(v = 1) + O_2(v = 1)$ | $7.00^{-10}$ | −120.0 | 560 | [a] |
| $CO(v = 3) + O_2(v = 0) \rightleftharpoons CO(v = 2) + O_2(v = 1)$ | $1.10^{-9}$ | −116.0 | 533 | [a] |
| $CO(v = 4) + O_2(v = 0) \rightleftharpoons CO(v = 3) + O_2(v = 1)$ | $1.40^{-9}$ | −112.0 | 506 | [a] |
| $CO(v = 1) + O_2(v = 1) \rightleftharpoons CO(v = 0) + O_2(v = 2)$ | $7.00^{-10}$ | −127.0 | 611 | [a] |
| $CO(v = 2) + O_2(v = 1) \rightleftharpoons CO(v = 1) + O_2(v = 2)$ | $1.40^{-9}$ | −124.0 | 584 | [a] |
| $CO(v = 3) + O_2(v = 1) \rightleftharpoons CO(v = 2) + O_2(v = 2)$ | $2.10^{-9}$ | −120.0 | 557 | [a] |
| $CO(v = 4) + O_2(v = 1) \rightleftharpoons CO(v = 3) + O_2(v = 2)$ | $2.10^{-9}$ | −116.0 | 530 | [a] |
| $CO(v = 1) + O_2(v = 2) \rightleftharpoons CO(v = 0) + O_2(v = 3)$ | $1.05^{-9}$ | −131.0 | 635 | [a] |
| $CO(v = 2) + O_2(v = 2) \rightleftharpoons CO(v = 1) + O_2(v = 3)$ | $2.10^{-9}$ | −127.0 | 608 | [a] |
| $CO(v = 3) + O_2(v = 2) \rightleftharpoons CO(v = 2) + O_2(v = 3)$ | $3.20^{-9}$ | −123.0 | 581 | [a] |
| $CO(v = 4) + O_2(v = 2) \rightleftharpoons CO(v = 3) + O_2(v = 3)$ | $4.20^{-9}$ | −119.0 | 554 | [a] |
| $CO(v = 1) + O_2(v = 3) \rightleftharpoons CO(v = 0) + O_2(v = 4)$ | $1.40^{-9}$ | −134.0 | 659 | [a] |
| $CO(v = 2) + O_2(v = 3) \rightleftharpoons CO(v = 1) + O_2(v = 4)$ | $2.80^{-9}$ | −130.0 | 633 | [a] |
| $CO(v = 3) + O_2(v = 3) \rightleftharpoons CO(v = 2) + O_2(v = 4)$ | $4.20^{-9}$ | −127.0 | 605 | [a] |
| $CO(v = 4) + O_2(v = 3) \rightleftharpoons CO(v = 3) + O_2(v = 4)$ | $5.60^{-9}$ | −123.0 | 579 | [a] |
| $CO(v = 1) + O_2(v = 4) \rightleftharpoons CO(v = 0) + O_2(v = 5)$ | $1.75^{-9}$ | −137.0 | 683 | [a] |
| $CO(v = 2) + O_2(v = 4) \rightleftharpoons CO(v = 1) + O_2(v = 5)$ | $3.50^{-9}$ | −134.0 | 657 | [a] |
| $CO(v = 3) + O_2(v = 4) \rightleftharpoons CO(v = 2) + O_2(v = 5)$ | $5.30^{-9}$ | −130.0 | 630 | [a] |
| $CO(v = 4) + O_2(v = 4) \rightleftharpoons CO(v = 3) + O_2(v = 5)$ | $7.00^{-9}$ | −126.0 | 603 | [a] |

[a]Extrapolated data from experiments.

equivalent to a $V$-$T, R$ process and is treated that way in the rate package.

$V$-$V$ energy transfer rates for $CO_2$-$O_2$ have not been included in the list of reactions in Table 4 because these rates have not been measured at high temperatures. The large energy defect ($\sim$800 cm$^{-1}$) is within a few wave numbers of that for $N_2$-$O_2$, and that process is known to be very slow. This rate cannot compete with $V$-$V$ transfer to CO or with the intramolecular $\nu_3$ loss process.

Intramolecular $V$-$V$ processes are listed in Table 5. As stated earlier, these near-resonant $V$-$V$ processes will be fast at the temperatures considered in this study. Unfortunately, none have been measured at high temperatures. The rate constants for this set of reactions are based on the experimental results for CO–CO at room temperature. These have an unusual defect dependence that was successfully reproduced by a theoretical model [12] incorporating both long- and short-range interactions. This model can be extended to high temperatures, for which the short-range interaction is dominant. The CO–CO rates in Table 5 are based on this calculation. There are room-temperature rate constants for $O_2$–$O_2$ [20], and the rate constants for high temperatures are scaled based on the short-range model of CO. A similar procedure was adopted for $CO_2(\nu_3)$ to obtain rates at high temperatures. The accuracy of these rate

**Table 5 Rate constants for intramolecular *V-V* processes**

| Reaction | $C$, cm$^3$/s | $\Delta E$, cm$^{-1}$ | Source |
|---|---|---|---|
| $CO(v = 1) + CO(v = 1) \rightleftharpoons CO(v = 0) + CO(v = 2)$ | $4.0^{-13}$ | 27 | [12] |
| $CO(v = 1) + CO(v = 2) \rightleftharpoons CO(v = 0) + CO(v = 3)$ | $6.0^{-13}$ | 54 | [a] |
| $CO(v = 1) + CO(v = 3) \rightleftharpoons CO(v = 0) + CO(v = 4)$ | $8.0^{-13}$ | 80 | [a] |
| $CO(v = 2) + CO(v = 2) \rightleftharpoons CO(v = 1) + CO(v = 3)$ | $1.2^{-12}$ | 27 | [a] |
| $CO(v = 2) + CO(v = 3) \rightleftharpoons CO(v = 1) + CO(v = 4)$ | $1.6^{-12}$ | 54 | [a] |
| $CO(v = 3) + CO(v = 3) \rightleftharpoons CO(v = 2) + CO(v = 4)$ | $2.4^{-12}$ | 27 | [a] |
| $CO_2(\nu_3 = 1) + CO_2(\nu_3 = 1) \rightleftharpoons CO_2(\nu_3 = 0) + CO_2(\nu_3 = 2)$ | $4.0^{-13}$ | 25 | [12] |
| $CO_2(\nu_3 = 1) + CO_2(\nu_3 = 2) \rightleftharpoons CO_2(\nu_3 = 0) + CO_2(\nu_3 = 3)$ | $6.0^{-13}$ | 50 | [a] |
| $CO_2(\nu_3 = 2) + CO_2(\nu_3 = 2) \rightleftharpoons CO_2(\nu_3 = 1) + CO_2(\nu_3 = 3)$ | $1.2^{-12}$ | 25 | [a] |
| $O_2(v = 1) + O_2(v = 1) \rightleftharpoons O_2(v = 0) + O_2(v = 2)$ | $4.0^{-13}$ | 24 | [20] |
| $O_2(v = 1) + O_2(v = 2) \rightleftharpoons O_2(v = 0) + O_2(v = 3)$ | $6.0^{-13}$ | 48 | [a] |
| $O_2(v = 1) + O_2(v = 3) \rightleftharpoons O_2(v = 0) + O_2(v = 4)$ | $8.0^{-13}$ | 72 | [a] |
| $O_2(v = 1) + O_2(v = 4) \rightleftharpoons O_2(v = 0) + O_2(v = 5)$ | $8.0^{-13}$ | 97 | [a] |
| $O_2(v = 2) + O_2(v = 2) \rightleftharpoons O_2(v = 1) + O_2(v = 3)$ | $1.2^{-12}$ | 24 | [a] |
| $O_2(v = 2) + O_2(v = 3) \rightleftharpoons O_2(v = 1) + O_2(v = 4)$ | $1.6^{-12}$ | 48 | [a] |
| $O_2(v = 2) + O_2(v = 4) \rightleftharpoons O_2(v = 1) + O_2(v = 5)$ | $2.0^{-12}$ | 72 | [a] |
| $O_2(v = 3) + O_2(v = 3) \rightleftharpoons O_2(v = 2) + O_2(v = 4)$ | $2.4^{-12}$ | 24 | [a] |
| $O_2(v = 3) + O_2(v = 4) \rightleftharpoons O_2(v = 2) + O_2(v = 5)$ | $3.0^{-12}$ | 48 | [a] |
| $O_2(v = 4) + O_2(v = 4) \rightleftharpoons O_2(v = 3) + O_2(v = 5)$ | $4.0^{-12}$ | 24 | [a] |

[a]Extrapolated data from experiments.

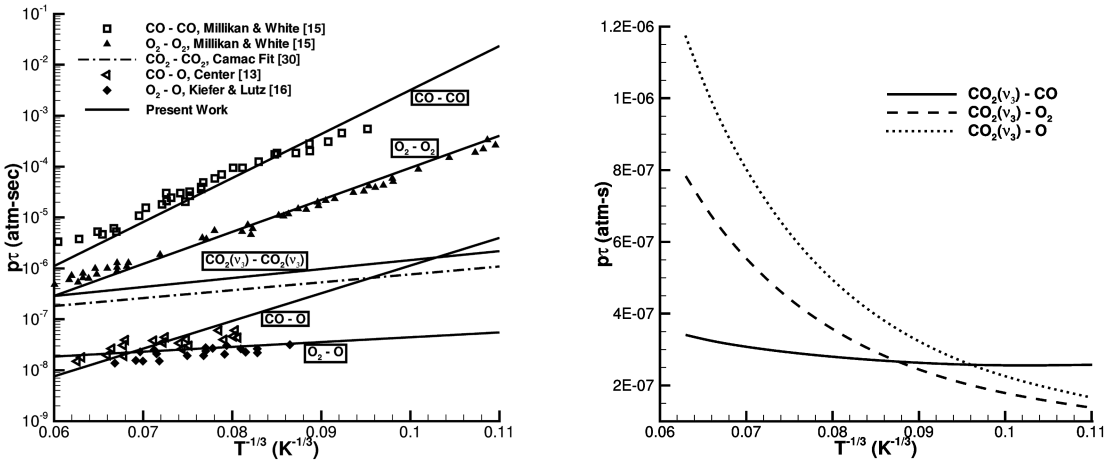


a) b)

**Fig. 1 Comparison of relaxation times.**

constants can be off by as much as a factor of 2, but because these processes are all fast enough, it does not really matter, and these processes do not take or release much energy into the translational or rotational degrees of freedom.

### C. Numerical Results

Numerical experiments were carried out to observe the variation of relaxation times with temperature. The relaxation time is defined as follows:

$$\frac{E_v - E_v^\star}{E_{v0} - E_v^\star} = e^{-t/\tau} \tag{8}$$

If $E_v$ is the vibrational energy at any time $t$, $E_v^\star$ is the equilibrium vibration energy at that particular temperature, and $E_{v0}$ is the initial vibrational energy, then the relaxation time can be defined as the time taken for the difference $E_v - E_v^\star$ to fall to $\frac{1}{e}(E_{v0} - E_v^\star)$ [23].

Figure 1a shows the comparison of the relaxation times with experiments. The solid lines represent the best-fit curve for the relaxation times obtained in the present work. The experimental data were obtained from [24]. The relaxation times of pairs of species such as CO–CO, CO–O, $O_2$–$O_2$, and $O_2$–O are in very good agreement with the experimental data. We see that separating the antisymmetric stretch levels from the symmetric stretch-bend levels leads to an increase in the relaxation time. The relaxation time can be related to the temperature for most pairs by the following equation:

$$p\tau = \exp(aT^{-\frac{1}{3}} + b) \text{ atm} \cdot \text{s} \tag{9}$$

The only exceptions to the preceding equation were the relaxation times for the pairs $CO_2(\nu_3)$–CO, $CO_2(\nu_3)$–$O_2$ and $CO_2(\nu_3)$–O. Figure 1b plots the variation of relaxation times with temperature. The following equation best describes the behavior:

$$p\tau = \frac{T^2 \exp(aT^{-\frac{1}{3}} + b)}{1 - \exp(-(\theta_v/T))} \text{ atm} \cdot \text{s} \tag{10}$$

where $\theta_v$ is the characteristic vibrational temperature of the antisymmetric stretch bend (3382 K). This shows that the product of pressure and relaxation time for $CO_2(\nu_3)$, when deactivated by CO, $O_2$, and O, decreases with decrease in temperature, and the relaxation time was also found to follow the same behavior. The values for constant $a$ and $b$ for different pairs are listed in Table 6.

In the next section we will discuss the chemistry and vibration coupling that we used to run the full-scale simulations.

## III. Chemistry—Vibration Coupling

Three reactions were identified to be necessary to adequately describe the chemistry in the $CO_2$–CO–$O_2$–O system:

$$CO_2 + M \rightleftharpoons CO + O + M \tag{11}$$

$$O_2 + M \rightleftharpoons O + O + M \tag{12}$$

$$CO_2 + O \rightleftharpoons CO + O_2 \tag{13}$$

One simple way of coupling chemistry and vibration is to use the modified values of the relaxation times from Table 6 and to use the Park [25] two-temperature model. The modified relaxation times are very similar to the Millikan and White [15] fits, except for $CO_2$. As mentioned before, the relaxation times for $CO_2(\nu_3)$ with CO, $O_2$, or O decrease with decrease in temperature. This model will be called model CV-$p\tau$.

Another way of coupling is to treat the problem as a two-step process. The first step would be to solve for the vibrational states from the rate data. The next step would be to sum up the number densities in these vibrational states, treat the chemistry reactions separately, and then redistribute the total number densities according to the Boltzmann distribution at the local gas kinetic temperature. This is not effective because it does not model the nonequilibrium in the flow and certainly does not allow population inversion in the vibrational states. So it was necessary to let individual vibrational states participate in the chemical reactions, even though this leads to an extensive set of possibilities. Because each vibrational state is considered to be a separate species, none of the standard vibration-dissociation models can be used here. Therefore, a way of combining the chemistry with the vibrational modes must be formulated.

**Table 6 Values of vibrational constants for $CO_2$, CO, and $O_2$**

| Colliding partners | $a$ | $b$ |
|---|---|---|
| | $CO_2$ | |
| $CO_2$ | 40.58 | −17.50 |
| CO | 77.01 | −36.75 |
| $O_2$ | 45.68 | −33.96 |
| O | 41.07 | −33.27 |
| | CO | |
| $CO_2$ | 9.53 | −15.45 |
| CO | 199.12 | −25.66 |
| $O_2$ | 116.76 | −20.53 |
| O | 125.25 | −26.21 |
| | $O_2$ | |
| $CO_2$ | 153.23 | −24.66 |
| CO | 162.71 | −25.01 |
| $O_2$ | 144.88 | −23.75 |
| O | 21.82 | −19.11 |

This chemistry–vibrational coupling model must reflect the following:

1) Species at higher vibrational states must show greater tendency to dissociate/react than the lower-lying states.

2) Detailed balance must be satisfied in the formulation (i.e., $k_f/k_b = K_{\text{eq}}$).

To understand the chemistry–vibration coupling used in the present work, let us consider a simple reaction:

$$A(v=i) + M \rightleftharpoons B(v=j) + M \tag{14}$$

where species $A$ at the $i$th vibrational level reacts with a collisional partner $M$ to give species $B$ at the $j$th vibrational level. We need to know the expressions for the equilibrium constant $K_{\text{eq}}^{A_iB_j}$ and the forward rate constant $k_f^{A_iB_j}$. But the data that we do know from literature is the rate constant and the equilibrium constant for the global chemical reaction comprising all of the vibrational states:

$$A + M \rightleftharpoons B + M \tag{15}$$

Let $k_f^{AB}$ be the forward rate constant and $K_{\text{eq}}^{AB}$ be the equilibrium constant for the reaction in Eq. (15). The backward rate constant is obtained by the principle of detailed balance.

We know the equilibrium constants for the following reactions:

$$A(v=0) \rightleftharpoons A(v=i) \qquad K_{\text{eq}}^{A_i} = \exp(-\Delta E_i^A/kT) \tag{16}$$

$$B(v=0) \rightleftharpoons B(v=j) \qquad K_{\text{eq}}^{B_j} = \exp(-\Delta E_j^B/kT) \tag{17}$$

where $\Delta E_i^A$ and $\Delta E_j^B$ denote the energy difference between the ground states of $A(v=0)$ and $B(v=0)$ and the excited states of $A(v=i)$ and $B(v=j)$, respectively.

To get the equilibrium constant for the reaction in Eq. (14), we need the equilibrium constant of the reaction between the ground states of $A$ and $B$:

$$A(v=0) + M \rightleftharpoons B(v=0) + M \tag{18}$$

which could then be combined with Eqs. (16) and (17) to yield the desired result.

The next step is to get the ground-state densities as a function of the total density and the temperature. As discussed in the previous section, the population $N_i$ for a given species in the level $i$ relative to that in the ground state $N_0$ is given by Eq. (1), and the total population in all of the states is given by Eq. (2). Because the statistical weights $g_i$ are unity for all the CO, $O_2$, and $CO_2$ antisymmetric stretch levels considered, the expression can be rewritten as

$$N_{\text{total}} = N_0(1 + \Sigma[\exp(-\Delta E_i/kT)]) \tag{19}$$

Further, the degree of anharmonicity at the temperatures considered is small, and so using the harmonic oscillator model, we can write

$$\Delta E_i = i\Delta E_0 = i\Delta E \tag{20}$$

With this assumption, it is then easy to do the summation in Eq. (19) as a geometric series (assuming infinite sum):

$$N_{\text{total}} = \frac{N_0}{1 - \exp(-\Delta E/kT)} \tag{21}$$

Applying this result to obtain a relationship between total density of $A$ and $A(v=0)$, and similarly for $B$ and $B(v=0)$, we get

$$[A] = \frac{[A(v=0)]}{1 - \exp(-\Delta E^A/kT)} \tag{22}$$

$$[B] = \frac{[B(v=0)]}{1 - \exp(-\Delta E^B/kT)} \tag{23}$$

where $[X]$ denotes the concentration of species $X$.

From Eqs. (22) and (23), the equilibrium constant for the reaction in Eq. (18) is

$$K_{\text{eq}}^{A_0B_0} = \frac{[B(v=0)]}{[A(v=0)]} = \frac{[B](1 - \exp(-\Delta E^B/kT))}{[A](1 - \exp(-\Delta E^A/kT))} = K_{\text{eq}}^{AB}\frac{1 - \exp(-\Delta E^B/kT)}{1 - \exp(-\Delta E^A/kT)} \tag{24}$$

Using the results derived previously, we can now obtain an expression for the equilibrium constant for the reaction in Eq. (14):

$$K_{\text{eq}}^{A_iB_j} = \frac{K_{\text{eq}}^{B_j}}{K_{\text{eq}}^{A_i}} K_{\text{eq}}^{A_0B_0} = \frac{\exp(-\Delta E_j^B/kT)(1 - \exp(-\Delta E^B/kT))}{\exp(-\Delta E_i^A/kT)(1 - \exp(-\Delta E^A/kT))} K_{\text{eq}}^{AB} \tag{25}$$

The expression for $K_{\text{eq}}^{AB}$ can be obtained from curve fits available in the literature.

Next, we need to obtain the rate constant $k_f^{A_iB_j}$ from the rate-constant expression for the global reaction $k_f^{AB}$. If we consider the classic description of the rate constant,

$$k_f = A_f^{rr} \exp\left(\frac{-E_{\text{act}}^f}{kT}\right) \tag{26}$$

where $A_f^{rr}$ is the preexponential factor, $E_{\text{act}}$ is the energy of activation, and $k$ is the Boltzmann constant. Based on this description, the rate constant $k_f$ [Eq. (26)] is basically the same as $k_f^{A_0B_0}$. The effect of higher vibrational states is to reduce the energy of activation and thereby increase the rate of the reaction. Using this simple model, we can derive the rate-constant expression for the reaction in Eq. (14) by altering the energy of activation as needed. The forward rate constant effectively takes the form

$$k_f^{A_iB_j} = A_f^{rr} \exp\left(\frac{-(E_{\text{act}}^f - \Delta E_i^A)}{kT}\right) = k_f^{A_0B_0} \exp\left(\frac{\Delta E_i^A}{kT}\right) \tag{27}$$

and similarly for the backward rate constant, we get

$$k_b^{A_iB_j} = A_b^{rr} \exp\left(\frac{-(E_{\text{act}}^b - \Delta E_j^B)}{kT}\right) = k_b^{A_0B_0} \exp\left(\frac{\Delta E_j^B}{kT}\right) \tag{28}$$

The preceding modification to the rate constants allows the higher vibrational states to have greater tendency to react than the low-lying states. Moreover, we also see that this derivation is consistent with the principle of detailed balance: that is,

$$K_{\text{eq}}^{A_iB_j} = \frac{k_f^{A_iB_j}}{k_b^{A_iB_j}} = \frac{k_f^{A_0B_0}}{k_b^{A_0B_0}} \frac{\exp(\Delta E_i^A/kT)}{\exp(\Delta E_j^B/kT)} = \frac{K_{\text{eq}}^{B_j}}{K_{\text{eq}}^{A_i}} K_{\text{eq}}^{A_0B_0} \tag{29}$$

[the same as Eq. (25)].

The next step is to find an expression that relates the rate constants $k_f^{A_0B_0}$ and $k_f^{AB}$. A nominal correction would be to relate the rate constants as follows:

$$k_f^{A_0B_0} = k_f^{AB}[1 - \exp(-\Delta E^A/kT)]^{-1} \tag{30}$$

$$k_b^{A_0B_0} = k_b^{AB}[1 - \exp(-\Delta E^B/kT)]^{-1} \tag{31}$$

so that the expressions are consistent with the derivation for the equilibrium constants.

We have outlined the basic principle in obtaining the rate constants and the equilibrium constants for the set of the reactions. It is easy to extend this derivation for reactions with multiple species such as Eq. (13). We will denote this way of coupling chemistry and vibration for all 16 species as model CV-16.

The expressions for the forward rate constants for the chemical reactions (Eqs. (11–13) are of the form

$$k_f = C_M \exp(-\theta/T) \tag{32}$$

**Table 7 Rate constants for the $CO_2$–CO–$O_2$–O system**

| $M$ | $C_M$, $cm^3/mol \cdot s$ | $\theta$, K | Source |
|---|---|---|---|
| *Dissociation reaction* $CO_2 + M \rightleftharpoons CO + O + M$ | | | |
| $CO_2$ | $2.2^{15}$ | 51,300 | [26] |
| CO | $9.4^{14}$ | 51,300 | [26] |
| $O_2$ | $9.4^{14}$ | 51,300 | [26] |
| O | $9.4^{14}$ | 51,300 | [26] |
| *Dissociation reaction* $O + O + M \rightleftharpoons O_2 + M$ | | | |
| $CO_2$ | $8.1^{13}$ | −890.6 | [27] |
| CO | $4.1^{13}$ | −890.6 | [27] |
| $O_2$ | $2.2^{13}$ | −890.6 | [27] |
| O | $2.2^{13}$ | −890.6 | [27] |
| *Exchange reaction* $CO_2 + O \rightleftharpoons CO + O_2$ | | | |
| —— | $2.5^{12}$ | 24,056 | [27] |

The rate constant for the backward reaction is obtained by the principle of detailed balance. The values of these constants are listed in Table 7. The equilibrium constants are evaluated using curve fits [28].

Both model CV-$p\tau$ and model CV-16 were used to run the full-scale simulations of the nozzle. The standard $CO_2$, which uses the Park [25] two-temperature model and the Landau—Teller model [29] for vibrational relaxation, is used to compare the models used in the present work. The Millikan and White [15] fits are used to obtain the relaxation times for all species except $CO_2$. Camac [30] rates are used for the vibrational relaxation of $CO_2$. Camac rates assume that all modes of $CO_2$ relax together.

## IV. Results and Discussion

### A. Nozzle Flowfield Computations

The coupled vibration—chemistry models were implemented in an axisymmetric CFD solver [31] to calculate the flowfield inside the nozzle. The CFD solver uses an excluded volume equation of state to account for the high-density effects inside the reservoir. For more information on the CFD solver, see [31]. The reservoir conditions are the same as in Table 2. An isothermal wall temperature of 300 K was assumed for the entire nozzle. The results are compared with the standard vibrational model for $CO_2$. To look at the differences in the flowfield prediction between the models, specific values are compared at the test-section location. Tables 8–10 show the comparison between the standard vibrational model and the models used in the present work.

Table 8 shows the comparison of the thermodynamic properties such as pressure, temperature, etc. The models used in the present work predict higher temperatures, pressures, and densities (and, therefore, lower Mach numbers) when compared with the standard model. The degree of vibrational nonequilibrium is very small for the standard model and model CV-$p\tau$. The chemical compositions of various species do not show much difference between the standard model and model CV-$p\tau$. The only difference between the standard model and model CV-$p\tau$ is the modified relaxation times. The vibrational relaxation in both the standard model and model CV-$p\tau$ is too fast to cause a vibrational nonequilibrium in the flow. Moreover, the fast relaxation times obtained for $CO_2(\nu_3)$ deactivation by CO, $O_2$, or O counter the effect of the slow relaxation of the antisymmetric mode of $CO_2$ during the expansion in the nozzle. This causes both the standard model and model CV-$p\tau$ to give similar results.

The chemistry–vibrational coupling used in model CV-16 predicts higher mass fraction of $CO_2$ and lower mass fractions of CO and $O_2$ (Table 9). This coupling effectively predicts a composition closer to chemical equilibrium than the other models. Because the stretch-bend modes were assumed to be in equilibrium with the translational and rotational modes, $T_v$ (stretch bend) is the same as $T$. The amount of vibrational energy stored can be understood by assigning a representative vibrational temperature $T_v^*$ to each of the species $CO_2(\nu_3)$, CO, and $O_2$. This vibrational temperature is calculated assuming the species to be a harmonic oscillator having the same amount of vibrational energy. These vibrational temperatures are listed in Table 10. These temperatures are purely representative of the vibrational energy content in the respective species. The vibrational temperatures for $CO_2(\nu_3)$, CO, and $O_2$ are higher than the translational temperature because of anharmonicity and should not be interpreted as the flow being in vibrational nonequilibrium. The number densities in the vibrational levels of $CO_2(\nu_3)$, CO, or $O_2$ were found to follow the Boltzmann distribution at a temperature close to the local translational temperature. Let us consider the amount of vibrational energy stored in the different species for the standard $CO_2$ model. By using the harmonic oscillator assumption, we can derive the total energy content in the species. This value for the standard $CO_2$ model is 0.2227 MJ/kg. A corresponding calculation for model CV-16 yields an energy content of 0.3425 MJ/kg in the vibrational modes. This model predicts a higher value for two reasons. First, the vibrational temperatures are larger than the standard model because of anharmonicity; second, the antisymmetric stretch modes of $CO_2$ are responsible for most of the vibrational energy, and because a higher mass fraction of $CO_2$ is predicted by model CV-16, the vibrational energy content is larger than the standard model. Even though the present model does predict higher vibrational energy content in the freestream, this is not close to the 42% of the total enthalpy value (2.5025 MJ/kg) recommended in [1]. To summarize, all of the models predict the flow to be close to vibrational equilibrium at the test section. Model CV-16 predicts a flow to be closer to chemical equilibrium than the other two models. In the next section we will look at the effect of these chemistry models on the shock standoff distance.

**Table 9 Mass fractions of species at the centerline test section**

| Chemistry model | $CO_2$ | CO | $O_2$ | O |
|---|---|---|---|---|
| Standard $CO_2$ model | .8629 | .0872 | .0497 | .000089 |
| Model CV-$p\tau$ | .8745 | .0798 | .0457 | 3.56E − 13 |
| Model CV-16 | .9384 | .0391 | .0225 | 3.64E − 08 |

**Table 10 Representative vibrational temperature of species at the centerline of the test section for model CV-16**

| Chemical species | $T_v^*$, K |
|---|---|
| $CO_2(\nu_3)$ | 1091.14 |
| CO | 1104.84 |
| $O_2$ | 1245.33 |

### B. Shock Standoff Studies

The simulations for the Mars Space Laboratory (MSL) shape are carried using a hybrid implicit unstructured finite volume solver (US3D) that solves the compressible Navier–Stokes equations [32]. The inviscid fluxes are calculated using a low dissipation version of Steger–Warming flux-vector splitting. Second-order accuracy in space is achieved using an upwind-biased MUSCL approach [33].

**Table 8 Centerline summary at the test section**

| Chemistry model | Density, $kg/m^3$ | Pressure, Pa | $T$, K | $T_v$, K | Mach |
|---|---|---|---|---|---|
| Standard $CO_2$ model | 0.00895 | 1613.88 | 892.68 | 895.69 (all) | 5.71587 |
| Model CV-$p\tau$ | 0.00933 | 1706.95 | 911.11 | 916.32 (all) | 5.68639 |
| Model CV-16 | 0.00933 | 1967.97 | 1082.30 | 1082.30 (stretch bend) | 5.41824 |

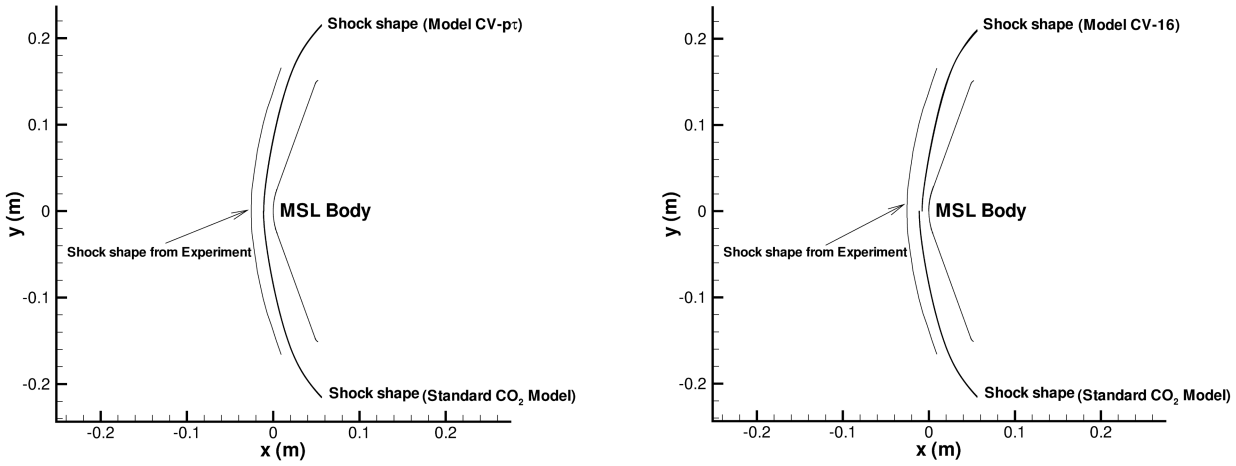


**Fig. 2 Comparison of shock shapes between standard model and a) model CV-$p\tau$ and b) model CV-16. Shock shape from experiment is indicated in Fig. 1.**

Time integration is performed implicitly using a parallel-line-relaxation procedure [34]. The MSL shape is a 31-cm-diam, 70 deg, sphere-cone geometry. The chemistry models, model CV-$p\tau$ and model CV-16, are coupled with the flow solver. The test-section conditions from the nozzle simulations (Tables 8 and 9) are used for the inflow. The grid used consists of 400 points along the surface and 163 points in the surface normal direction, with points clustered near the shock for better resolution. Isothermal catalytic wall temperature of 300 K is used for the wall. The experimental shock shape is extracted from the schlieren data in [1]. The shock shape from simulation is obtained from the location of the maximum temperature gradient. These extracted shock shapes are shown in Fig. 2.

Figure 2a compares model CV-$p\tau$ with the standard $CO_2$ model. The inflow conditions are very close to vibrational equilibrium for both the models and the extent of chemical nonequilibrium is also the same, and so the shock standoff distance does not change between the models. Figure 2b shows the comparison between model CV-16 and the standard $CO_2$ model. From the nozzle simulations, we know that model CV-16 predicts the flow at the test section to be closer to chemical equilibrium than the standard model. This is reflected in the shock standoff calculations. The study by Maclean and Holden [1] shows the shock standoff distance to decrease when the composition at the test section is closer to chemical nonequilibrium, and because model CV-16 predicts a composition closer to chemical equilibrium, the shock standoff distance is smaller despite a lower Mach number. We also see that the shock standoff distance is sensitive to the chemistry–vibration coupling model.

## V. Conclusions

A state-specific vibrational model for $CO_2$, CO, $O_2$, and O involving 16 species was formulated and validated against experiments. The antisymmetric stretching mode was decoupled from the symmetric stretching and the bending modes. The symmetric stretching and the bending modes were assumed to be in equilibrium with the translational mode. Results show that the antisymmetric mode relaxes slower than the other two modes. Additionally, it was also found that the relaxation times for the collisional deactivation of $CO_2(\nu_3)$ by CO, $O_2$, and O increases with increase in temperature.

Two methods of chemistry–vibrational coupling were used to the nozzle expansion. The numerical experiments of the vibrational model were used to generate curve fits for the relaxation times. These curve fits were used with a standard chemistry–vibration model for a reduced set of the main four species. This model gave results similar to the standard model for both the nozzle test-section conditions and the shock standoff distance. The other method included all 16 state-specific species and a full calculation based on rate expressions for every possible reaction between the species. This method predicted a flow closer to chemical equilibrium at the test section than other models, thereby estimating a decreased shock standoff distance. All models showed that the flow at the test section is close to vibrational equilibrium. The present work used an advanced state-specific vibrational model that considered the antisymmetric mode separately from the other two modes of $CO_2$. This approach does not explain the phenomenon of increased shock standoff distance observed in the LENS CUBRC facility.

## References

[1] MacLean, M., and Holden, M., "Numerical Assessment of Data in Catalytic and Transitional Flows for Martian Entry," AIAA Paper 2006-2946, June 2006.

[2] Taylor, R. L., and Bitterman, S., "Survey of Vibrational Relaxation Data for Process Important in the $CO_2$-$N_2$ Laser System," *Reviews of Modern Physics*, Vol. 41, No. 1, 1969, pp. 26–47.

[3] Lewis, P. F., and Trainor, D. W., "Survey of Vibrational Relaxation Data for $O_2$, $N_2$, NO, $H_2$, CO, HF, HCl, $CO_2$, and $H_2O$," AVCO Everett Research Lab., Rept. Amp-422, Everett, MA, Nov. 1974.

[4] Weitz, E., and Flynn, G. W., "Laser Studies of Vibrational and Rotational Relaxation in Small Molecules," *Annual Review of Physical Chemistry*, Vol. 25, 1974, pp. 275–315.

[5] Ono, S., and Teii, S., "Vibrational Temperature in a Weakly Ionised $CO_2$-$N_2$-He Discharge," *Journal of Physics D: Applied Physics*, Vol. 18, No. 3, 1985, pp. 441–450.

[6] Jacobs, R. R., Pettipiece, K. J., and Thomas S. J., "Rate Constants for the $CO_2$ $02^0$2-$10^0$0 Relaxation," *Physical Review A*, Vol. 11, No. 1, 1975, pp. 54–61.

[7] Orr, B. J., and Smith, I. W. M., "Collision-Induced Vibrational Energy Transfer in Small Polyatomic Molecules," *Journal of Chemical Physics*, Vol. 91, 1987, pp. 6106–6119.

[8] Lunt, S. L., Jones, C. T. W., and Simpson, C. J. S. M., "Rate Constants for the Deactivation of the 15 m Band of Carbon Dioxide by the Collision Partners $CH_3F$, $CO_2$, $N_2$, Ar and Kr over the Temperature Ranges 300 to 150 K," *Chemical Physics Letters*, Vol. 115, No. 1, 1985, pp. 60–65.

[9] Lopez-Valverde, M. A., and Lopez-Puertas M., "A Non-local Thermodynamic Equilibrium Radiative Transfer Model for Infrared Emission in the Atmosphere of Mars," *Journal of Geophysical Research*, Vol. 99, No. 6, 1994, pp. 13,117–13,132.

[10] Limbaugh, C., and Drakes, J., "$CO_2$ Vibrational Relaxation Effects in a Laser-Heated Hypersonic Flow," AIAA Paper 1997-2492, June 1997.

[11] Rapp, D., and Kassal, T., "The Theory of Vibrational Energy Transfer Between Simple Molecules in Nonreactive Collisions," *Chemical Reviews (Washington, DC)*, Vol. 69, No. 1, 1969, pp. 61–102.

[12] Jeers, W. Q., and Kelley, J. D., "Calculations of *V-V* Transfer Probabilities in CO–CO Collisions," *Journal of Chemical Physics*, Vol. 55, No. 9, 1971, pp. 4433–4437.

[13] Center, R. E., "Vibrational Relaxation of CO by O Atoms," *Journal of Chemical Physics*, Vol. 58, No. 12, 1973, pp. 5230–5236.

[14] Lewittes, M. E., Davis, C. E., and McFarlane, R. A., "Vibrational Deactivation of CO ($v = 1$) by Oxygen atoms," *Journal of Chemical Physics*, Vol. 69, No. 5, 1978, pp. 1952–1957.
[15] Millikan, R. C., and White, D. R., "Systematics of Vibrational Relaxation," *Journal of Chemical Physics*, Vol. 39, No. 12, 1963, pp. 3209–3213.
[16] Kiefer, J. H., and Lutz, R. W., *11th Combustion Symposium*, Combustion Inst., Pittsburgh, PA, 1966, p. 67.
[17] Breen, J. E., Quy, R. B., and Glass, G. P., "Vibrational Relaxation of $O_2$ in the Presence of Atomic Oxygen," *Journal of Chemical Physics*, Vol. 59, No. 1, 1973, pp. 556–557.
[18] Starr, D. F., and Hancock, J. K., "Vibrational Energy Transfer in CO-$CO_2$ Mixtures from 163 to 406 K," *Journal of Chemical Physics*, Vol. 63, No. 12, 1975, pp. 4730–4734.
[19] Taylor, R. L., "Tables of Rate and Photochemical Data for Modeling of the Stratosphere," *Chemical Kinetics Data Survey, 7*, National Bureau of Standards, Rept. NBSIR 74-430, revised ed., 1974.
[20] Ahn, T., Adamovich, I., and Lempert, W. R., "Stimulated Raman Scattering Measurements of *V-V* Transfer in Oxygen," *Chemical Physics*, Vol. 323, No. 2, 2006, pp. 532–544.
[21] Herzberg, G., *Infrared and Raman Spectra*, Vol. 1, Van Nostrand, New York, 1st ed., 1947.
[22] Herzberg, G., *Spectra of Diatomic Molecules*, Vol. 1, 1st ed., Van Nostrand, New York, 1959.
[23] Vincenti, W. G., and Kruger, C. H., *Introduction to Physical Gas Dynamics*, Krieger, Malabar, FL, 1965, p. 203.
[24] Park, C., Howe, J. T., Jae, R. L., and Candler, G. V., "Review of Chemical-Kinetic Problems of Future NASA Missions, 2: Mars Entries," *Journal of Thermophysics and Heat Transfer*, Vol. 8, No. 1, 1994, pp. 9–23.
[25] Park, C., *Nonequilibrium Hypersonic Aerothermodynamics*, Wiley, New York, 1990.
[26] Oehlschlaeger, M. A., "Shock Tube Studies of Thermal Decomposition Reactions Using Ultraviolet Absorption Spectroscopy," Ph.D. Thesis, Stanford Univ., Stanford, CA, June 2005.
[27] Warnatz, J., *Combustion Chemistry: Rate Coefficients in the C/H/O System*, Springer–Verlag, New York, 1984.
[28] Mitcheltree, R. A., and Gnoo, P. A., "Wake Flow About a MESUR Mars Entry Vehicle," AIAA Paper 1994-1958, June 1994.
[29] Landau, L., and Teller, E., "Zur Theorie der Schalldispersion," *Physikalische Zeitschrift der Sowjetunion*, Vol. 10, No. 1, 1936, p. 34.
[30] Camac, M., "$CO_2$ Relaxation Processes in Shock Waves," *Fundamental Phenomena in Hypersonic Flows*, Cornell Univ. Press, New York, 1966, pp. 195–215.
[31] Candler, G. V., "Hypersonic Nozzle Analysis Using an Excluded Volume Equation of State," AIAA Paper 2005-5202, June 2005.
[32] Nompelis, I., Drayna, T. W., and Candler, G. V., "Development of Hybrid Unstructured Implicit solver for the Simulation of Reacting Flows over Complex Geometries," AIAA Paper 2004-227, 2004.
[33] Nompelis, I., Drayna, T. W., and Candler, G. V., "A Parallel Unstructured Implicit Solver for Hypersonic Reacting Flow Simulations," AIAA Paper 2005-4867, June 2005.
[34] Wright, M. J., Candler, G. V., and Bose, D., "Data-Parallel Line Relaxation Method for the Navier Stokes Equations Using Gauss-Seidel Line Relaxation," *AIAA Journal*, Vol. 36, No. 9, 1998, pp. 1603–1609.